

# Group-velocity dispersion engineering of tantalum integrated photonics

JENNIFER A. BLACK,<sup>1,\*</sup> RICHELLE STREATER,<sup>1,2</sup> KIERAN F. LAMEE,<sup>1,2</sup> DAVID R. CARLSON,<sup>1</sup> SU-PENG YU,<sup>1,2</sup> SCOTT B. PAPP<sup>1,2</sup>

<sup>1</sup>Time and Frequency Division, National Institute of Standards and Technology, Boulder, Colorado 80305, USA

<sup>2</sup>Department of Physics, University of Colorado, Boulder, CO 80309, USA

\*Corresponding author: jennifer.black@nist.gov

Received XX Month XXXX; revised XX Month, XXXX; accepted XX Month XXXX; posted XX Month XXXX (Doc. ID XXXXX); published XX Month XXXX

**Designing integrated photonics, especially to leverage Kerr-nonlinear optics, requires accurate and precise knowledge of refractive index across the visible to infrared spectral ranges. Tantalum (Ta<sub>2</sub>O<sub>5</sub>) is an emerging material platform for integrated photonics and nanophotonics that offers broadband ultralow loss, moderately high nonlinearity, and advantages for scalable and heterogeneous integration. We present refractive-index measurements on a thin film of tantalum, and we explore the efficacy of this data for group-velocity dispersion (GVD) engineering with waveguide and ring-resonator devices. In particular, the observed spectral extent of supercontinuum generation in fabricated waveguides, and the wavelength dependence of free spectral range (FSR) in optical resonators provide a sensitive test of our integrated-photonics design process. Our work opens up new design possibilities with tantalum, including with octave-spanning soliton microcombs.**

<http://dx.doi.org/10.1364/OL.99.099999>

Photonic-integrated circuits (PICs) of waveguide-based devices offer breakthrough opportunities for basic scientific investigations, applications with light-matter interactions, and commercial devices that are widely used. In particular, waveguide PICs provide tight optical confinement and GVD engineering that is ideal for nonlinear optics. Through the Kerr effect, PIC designers may leverage efficient wavelength conversion at low input power [1], generation of chip-scale optical-frequency combs [2], and ultrabroad bandwidth supercontinuum [3]. Several materials are suitable for nanophotonic nonlinear device design [4–7]. Silicon nitride has attracted attention as a complementary metal-oxide-semiconductor (CMOS) compatible  $\chi^{(3)}$  nonlinear material with nonlinear index,  $n_2 = 2.4 \times 10^{-19} \text{ m}^2/\text{W}$  [8], an order of magnitude greater than silicon dioxide [9]. Broadband knowledge of silicon nitride's optical properties enables the precise GVD engineering necessary for successful device design [10]. As a result, silicon-

nitride devices have generated chip-scale supercontinua spanning an octave or more [11,12] as well as chip-scale octave-spanning Kerr soliton optical frequency combs [13].

Here, we explore the refractive index and the GVD design space of tantalum pentoxide (Ta<sub>2</sub>O<sub>5</sub>, hereafter tantalum), a promising, CMOS-compatible  $\chi^{(3)}$  nonlinear material. Indeed, tantalum offers superior material properties than silicon nitride, including a slightly higher nonlinear index  $n_2 = 6.2 \times 10^{-19} \text{ m}^2/\text{W}$ , much lower residual stress (38 MPa), a smaller thermo-optic coefficient ( $8.8 \times 10^{-6} \text{ 1/K}$ ), and a broader transparency window [14,15]. These factors, tantalum's high index of refraction, and tantalum's low temperature processing requirement make it an important integrated-photonics platform for linear [16,17] and nonlinear applications [18–21].

Obtaining an accurate and precise understanding of the bulk material properties is critical for future PIC design, particularly using the ion-beam-sputtered tantalum films that our previous work has shown offers low-loss [14]. Previous reports of the index of refraction and absorption coefficient are available up to a wavelength of 1.8  $\mu\text{m}$  [15,22], but provide inconsistent results, making it challenging to accurately design tantalum PICs. To better understand tantalum's optical properties and to extend this information into the mid-infrared, we have measured the refractive index and absorption coefficient. We deposited an 800 nm-thick tantalum layer on 3  $\mu\text{m}$ -thick thermally oxidized silicon wafer, and J. A. Woollam Co. [23] measured the layer across the spectral ranges of 190 – 1700 nm and 1.7 – 39.2  $\mu\text{m}$  using RC2 and IR-VASE ellipsometry instruments, respectively. The data were fit simultaneously across both spectral regions using a combination of Sellmeier, Tauc-Lorentz, and several Gaussian dispersion functions. Figure 1(a) shows the real index of refraction ( $n$ ) and extinction coefficient ( $k$ ) of tantalum as a function of wavelength ( $\lambda$ ) from 200 nm to 10  $\mu\text{m}$ , where the complex index of refraction,  $\tilde{n} = n + i \cdot k$ . In this spectral region, the real index of refraction is predominantly larger than 2, which provides a relatively large refractive index contrast with common cladding materials (e.g. air and silicon dioxide), and the absorption coefficient is relatively low over the range 320 nm to 8  $\mu\text{m}$ . Eq. 1 presents a third-order Sellmeier equation fit

$$(1) n^2 = 1 + \frac{0.033\lambda^2}{\lambda^2 - 0.368^2} + \frac{3.212\lambda^2}{\lambda^2 - 0.1639^2} + \frac{3.747\lambda^2}{\lambda^2 - 14.5^2}$$

describing the real index of refraction data from 500 nm to 5  $\mu\text{m}$ . The root-mean-square error of the fit is 0.00057.

Using Eq. 1 as input to finite-element electromagnetic field simulations of nanophotonic waveguides, we calculate the GVD of various cross-sectional geometries of tantala PIC geometries. Figure 1(b) presents a survey of calculated GVD for straight tantala waveguide cross-sectional geometries. The simulated waveguides are a tantala core on silicon dioxide with top and side air-cladding and cross-sectional dimensions of thickness ( $t$ ) and width ( $w$ ). Varying the thickness and width of the waveguides makes possible anomalous GVD in various spectral regions. Figure 1(b) shows simulated waveguide thickness from 500 nm to 1750 nm, demonstrating anomalous GVD for light polarized in the chip-plane from the near-infrared into the mid-infrared, and we find that anomalous GVD is possible for straight waveguides with thicknesses of 350 nm and larger, supporting anomalous GVD at a minimum wavelength of  $\sim 770$  nm.

Using the GVD information, we design and fabricate both supercontinuum-generation waveguides and ring resonators. We fabricate the devices by electron-beam lithography and plasma etching of a tantala layer deposited on a thermally oxidized silicon wafer. The top cladding is air, though an oxide cladding is possible [21]. A deep-reactive-ion etch dices the wafer into chips and an inverse taper to the edge of the devices enhances the fundamental mode overlap for coupling optimization from a lensed fiber [24]. The loss per facet is 3.4 dB and the waveguide propagation losses are as low as 0.1 dB/cm [21]. In this paper, we test Eq. 1 with experiments that are highly GVD sensitive, namely the spectral extent of supercontinuum generation and the wavelength dependence of FSR in ring resonators. Our results indicate that design of tantala PICs or nonlinear devices are within fabrication tolerances across multiple wafer runs.

PIC waveguides with high nonlinearity are ideal for supercontinuum generation with an input pulsed laser [25]. For comparison, highly nonlinear optical fibers are often used to

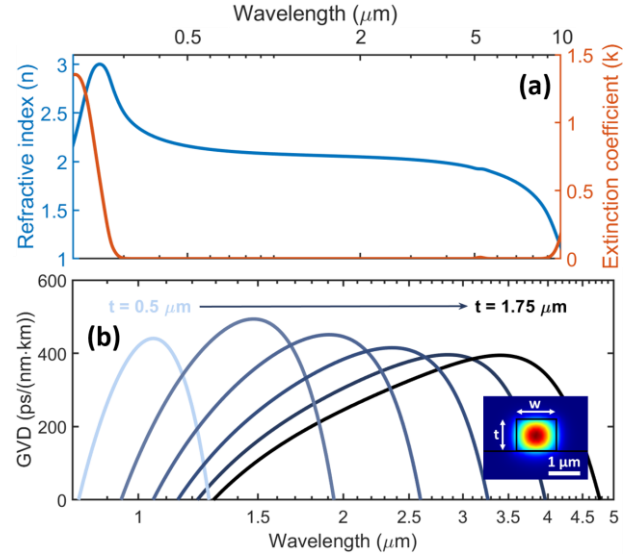


Fig. 1. (a) Refractive index ( $n$ ) and extinction coefficient ( $k$ ) data for tantala from 200 nm to 10  $\mu\text{m}$  on a log wavelength scale. A broad transparency window is evident from 320 nm to 8  $\mu\text{m}$ . (b) The simulated GVD for various straight tantala waveguide geometries as a function of wavelength from 800 nm to 5  $\mu\text{m}$ . The waveguide thickness  $t$  varies from 0.5 to 1.75  $\mu\text{m}$  in 0.25  $\mu\text{m}$  steps and the waveguide width  $w$  is a constant factor 1.25 times the thickness,  $w = 1.25 \times t$ . The inset shows a simulation ( $t = 1 \mu\text{m}$ ) of the fundamental transverse-electric mode with labelled cross-section dimensions ( $t \times w$ ).

achieve such spectral broadening in silica [26]. However, PIC waveguides offer much higher nonlinearity, design flexibility, and importantly geometrically tunable GVD [25]. We design and fabricate several tantala supercontinuum waveguides on silicon dioxide with a top and side air-cladding, a waveguide thickness of 570 nm and an optical path length of 15 mm. We design the devices

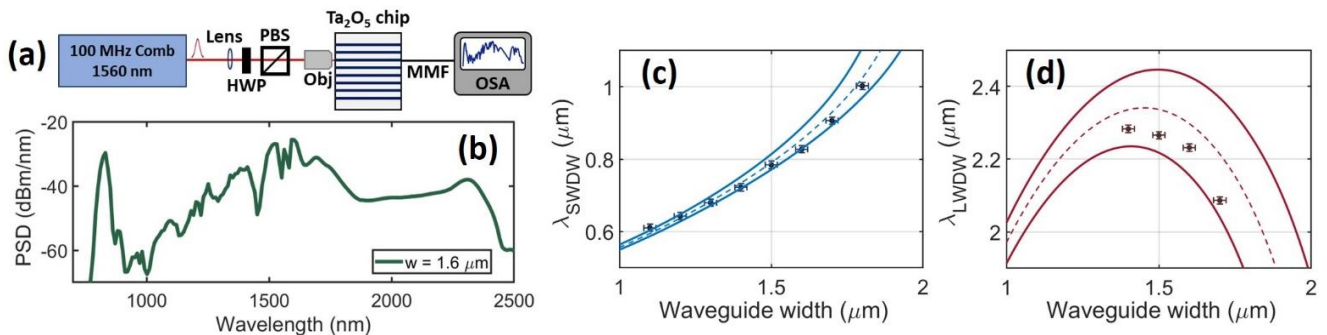


Fig. 2. (a) Experimental setup for supercontinuum measurements. A 100 MHz repetition rate optical frequency comb operating at 1560 nm ( $< 100$  mW average power) pumps the tantala device ( $\text{Ta}_2\text{O}_5$  chip). A half-wave plate (HWP) and polarizing beam splitter (PBS) prepare the optical power and polarization before the chip. A high-numerical-aperture aspheric lens (Obj) launches light onto the device, a multi-mode optical fiber (MMF) collects the transmitted light and an optical spectrum analyzer (OSA) monitors the output spectrum. (b) A sample supercontinuum spectrum (power spectral density, PSD) vs wavelength for waveguide width  $w = 1.6 \mu\text{m}$ . The average input pump power is 90 mW (pulse energy of 0.9 nJ). Measured zero-power dispersive wave wavelengths, (c)  $\lambda_{\text{SWDW}}$  and (d)  $\lambda_{\text{LWDW}}$  for various waveguide widths. The data (points) agree with our simulations within fabrication tolerances; dashed line is the target geometry and solid lines denote  $\pm 10$  nm thickness variation.

to offer anomalous GVD in the 1550 nm region and two zero-GVD wavelengths for dispersive wave generation on the short- and long-wavelength side of the pump. To determine the accuracy of our GVD data, we compare the dispersive wave wavelengths of our supercontinuum spectra with theory. The peak wavelength of the dispersive waves depends sensitively on the waveguide GVD and the optical pump power [27,28]. To remove the pump power dependence, we use a power scan technique to record the supercontinuum spectra as a function of pump power in order to extract the zero-pump power short and long-wavelength dispersive wave wavelengths ( $\lambda_{\text{SWDW}}$  and  $\lambda_{\text{LWDW}}$ ). To vary the GVD, we fabricate several waveguide widths (1.1 to 1.9  $\mu\text{m}$ ).

Figure 2(a) presents a schematic of the experimental setup. We use a 100 MHz repetition rate mode-locked laser with 80 fs-duration pulses at a central wavelength of 1560 nm. We couple light into the device with a microscope objective and collect the output from the chip with a multi-mode optical fiber which directs the transmitted light to an optical spectrum analyzer. The fabricated devices demonstrate low optical power dispersive wave wavelength generation. Figure 2(b) shows a sample spectrum collected from a device with waveguide width of 1.6  $\mu\text{m}$ , pumped with an average input pump power of 90 mW (pulse energy 0.9 nJ). We find  $\lambda_{\text{SWDW}}$  and  $\lambda_{\text{LWDW}}$  by extrapolating a fit of the pump power dependent dispersive wave wavelengths. Figure 2(c) and 2(d) present  $\lambda_{\text{SWDW}}$  and  $\lambda_{\text{LWDW}}$  as a function of supercontinuum waveguide width. A semi-vectorial method is used to simulate the GVD of the various waveguides to model  $\lambda_{\text{SWDW}}$  and  $\lambda_{\text{LWDW}}$ . The zero-GVD wavelengths are consistent with the predicted dispersive

wave wavelengths at low pump powers in the nonlinear Schrödinger equation [29].

The experimental (dots) and simulated (lines) results are in good agreement. The dashed lines represent the target geometry (waveguide thickness of 570 nm with various waveguide width) and the solid lines signify a variation of  $\pm 10$  nm in the waveguide thickness, demonstrating agreement within fabrication tolerances. More complex GVD designs using multi-segment waveguides [30] or suspended structures [6] to prevent silica cladding absorption at longer wavelengths [21] can increase the supercontinuum bandwidth.

Ring resonators enhance the intensity of optical fields and provide a discrete set of propagation momenta. Ring resonators are useful for sensitive detection of bioparticles [31] and nonlinear processes, such as four-wave mixing and optical parametric oscillation [32], wavelength translation [1], and soliton optical-frequency-comb generation [2]. To test Eq. 1, we fabricate tantala ring resonators and characterize the wavelength dependence of their FSR. In particular, the integrated dispersion

$$(2) \quad D_{\text{int}}(\mu) = \nu_{\mu} - (\nu_0 + \text{FSR} \times \mu)$$

is a polynomial expansion of the FSR as a function of azimuthal mode  $\mu$  with respect to a reference optical frequency  $\nu_0$  [2]. We calculate  $D_{\text{int}}$  using a finite-element-method (FEM) mode solver of a tantala ring resonator, including the specific tantala layer thickness, ring resonator waveguide width (RW), and ring radius (RR). We have determined that post-fabrication scanning-electron microscope images of the waveguide facets at chip edge are critical to understand the fabricated cross-sectional geometry as compared to the target design. Indeed, our current dry-etching recipe, while providing smooth and vertical sidewalls, results in a 50 nm-thick tantala residual pedestal, which we include in our FEM simulations to increase accuracy.

Figure 3 presents measurements of  $D_{\text{int}}$  versus the resonator azimuthal number as defined in Eq. 2 for several 200 GHz-FSR ring resonators with a RR of 112.5  $\mu\text{m}$ , measured to the center of the ring resonator waveguide. The devices have typical loaded quality factors of  $1 \times 10^6$ . We use lensed fibers to launch light into the on-chip coupling waveguide and to collect light after the resonator. Using a wavelength-tunable, narrow-linewidth, continuous-wave laser and a wavelength meter (Fig. 3a), we record the resonant frequencies of as many fundamental transverse-electric modes as possible (Fig. 3b); we determine the resonant frequency by the minimum of resonator laser transmission. We explore the wavelength range of 1510–1620 nm. Fig. 3b presents  $D_{\text{int}}$  measurements (color-coded open circles) and simulations (color-coded lines) for four specific settings of RW, namely 1625 nm (blue), 1775 nm (orange), 1925 nm (yellow), and 2075 nm (purple) that are designed to tune the GVD from anomalous to normal. In these data, degeneracies with higher-order transverse modes of the ring resonator perturb the otherwise monotonic behavior about  $\mu = 0$ . These results demonstrate the efficacy and accuracy of geometric GVD engineering in tantala for various applications.

Lastly, we present designs for octave-bandwidth soliton microcombs in 1 THz-FSR resonators, which we can fabricate; see the image in Fig. 3(c). These designs require a high level of GVD engineering and are a benchmark of soliton microcombs as the octave-bandwidth spectra provide f-2f referencing which is critical for stabilizing the comb [13]. We explore the theoretical design of octave-bandwidth 1 THz-FSR tantala resonators (RR = 21.25  $\mu\text{m}$ )

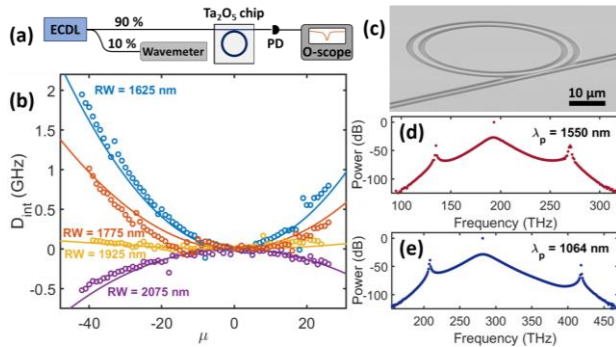


Fig. 3. (a) Schematic of the experimental setup. A widely tunable external cavity diode laser (ECDL) probes the tantala ring resonator ( $\text{Ta}_2\text{O}_5$  chip). A fiber coupler sends 10 % of the optical power to a wavelength meter (wavelength meter) for optical frequency measurement. A photodetector (PD) monitors the laser light transmitted through the ring resonator. Lensed fibers launch light into the device and collect light from the device. (b) The integrated dispersion ( $D_{\text{int}}$ , Eq. 2) with pump wavelength near 1550 nm for 200 GHz-FSR (RR = 112.5  $\mu\text{m}$ ) with ring widths 1625, 1775, 1925 and 2075 nm. The data (circles) and simulation (lines) are in good agreement. (c) A scanning electron microscope image of a ring resonator with 1 THz-FSR (RR = 22.5  $\mu\text{m}$ ). LLE simulation of an octave-spanning optical frequency comb with pump wavelength (d) 1550 nm (193.4 THz) and (e) 1064 nm (281.8 THz). The ring resonator dimensions,  $t \times w$ , are 570 nm  $\times$  1560 nm (415 nm  $\times$  737 nm) for pump wavelength 1550 (1064) nm and RR = 21.25  $\mu\text{m}$ .

for two commonly available pump wavelengths in the infrared, 1550 nm and 1064 nm. Both have been used to demonstrate soliton optical frequency Kerr comb generation with 1-THz-FSR devices in silicon nitride [13,33]. Our design procedure uses FEM simulations to choose a waveguide geometry based on our experience of how  $D_{\text{int}}$  will affect the soliton spectrum. We use the Lugiato-Lefever equation (LLE) to confirm and refine the choice of geometry [34]. We find the ring resonator waveguide cross-sectional dimensions for octave-spanning soliton frequency combs to be  $t \times RW = 570 \text{ nm} \times 1560 \text{ nm}$  for the 1550 nm pump wavelength and  $415 \text{ nm} \times 737 \text{ nm}$  for the 1064 nm pump wavelength. Figure 3(d) and 3(e) present the LLE simulated output soliton optical frequency comb spectra for pump wavelengths of 1550 and 1064 nm, respectively. We model the pump mode as critically coupled with a loaded quality factor of  $1 \times 10^6$ , and the on-chip optical pump power is forty times the optical parametric oscillation threshold [34]. The peak power of modes near the zero-GVD crossing (dispersive waves) reside at 134.9 and 270.1 THz for the 1550 nm (193.4 THz) pump and 208.7 and 418.2 THz for the 1064 nm (281.8 THz) pump.

In conclusion, we have presented broadband refractive index and extinction coefficient data for tantalum. The material provides a broad transparency window from the ultraviolet to the mid-infrared, a high index of refraction and a large nonlinearity making it an ideal candidate for fabricating linear and nonlinear integrated photonic devices. We provide an analytic third-order Sellmeier equation whose accuracy we verified by its use in designing several chip-scale nonlinear photonic devices. Anomalous GVD is possible from the near- to mid-infrared. We presented octave-spanning supercontinuum waveguides with both short and long wavelength dispersive waves and find good agreement between the experimental and simulated results. Additionally, we presented ring resonators with integrated dispersions well predicted by modelling. We show that octave-spanning soliton frequency combs are possible for pump wavelengths 1064 and 1550 nm.

**Funding.** This work was supported by NIST, DARPA A-PhI, and Advanced Research Projects Agency-Energy (ARPA-E), U.S. Department of Energy, under Award Number DE-AR0001042 program. JAB acknowledges support from the NRC Postdoctoral Fellowship.

**Acknowledgment.** We thank Pablo Acedo and Zachary Newman for technical review of the paper. We thank Ramin Lalezari for helpful information.

**Disclosures.** David Carlson is co-founder of Octave Photonics. The remaining authors do not currently have a financial interest in tantalum integrated photonics.

## REFERENCES

- X. Lu, G. Moille, Q. Li, D. A. Westly, A. Singh, A. Rao, S.-P. Yu, T. C. Briles, S. B. Papp, and K. Srinivasan, *Nature Photonics* **13**, 593 (2019).
- T. J. Kippenberg, A. L. Gaeta, M. Lipson, and M. L. Gorodetsky, *Science* **361**, (2018).
- A. S. Mayer, A. Klenner, A. R. Johnson, K. Luke, M. R. E. Lamont, Y. Okawachi, M. Lipson, A. L. Gaeta, and U. Keller, *Opt. Express*, OE **23**, 15440 (2015).
- B. Kuyken, T. Ideguchi, S. Holzner, M. Yan, T. W. Hänsch, J. Van Campenhout, P. Verheyen, S. Coen, F. Leo, R. Baets, G. Roelkens, and N. Picqué, *Nature Communications* **6**, 6310 (2015).
- D. D. Hickstein, H. Jung, D. R. Carlson, A. Lind, I. Coddington, K. Srinivasan, G. G. Ycas, D. C. Cole, A. Kowligy, C. Fredrick, S. Droste, E. S. Lamb, N. R. Newbury, H. X. Tang, S. A. Diddams, and S. B. Papp, *Phys. Rev. Applied* **8**, 014025 (2017).
- D. Yoon Oh, K. Y. Yang, C. Fredrick, G. Ycas, S. A. Diddams, and K. J. Vahala, *Nature Communications* **8**, 13922 (2017).
- B. Kuyken, M. Billet, F. Leo, K. Yvind, and M. Pu, *Opt. Lett.*, OL **45**, 603 (2020).
- K. Ikeda, R. E. Saperstein, N. Alic, and Y. Fainman, *Opt. Express*, OE **16**, 12987 (2008).
- K. S. Kim, R. H. Stolen, W. A. Reed, and K. W. Quoi, *Opt. Lett.*, OL **19**, 257 (1994).
- K. Luke, Y. Okawachi, M. R. E. Lamont, A. L. Gaeta, and M. Lipson, *Opt. Lett.*, OL **40**, 4823 (2015).
- A. R. Johnson, A. S. Mayer, A. Klenner, K. Luke, E. S. Lamb, M. R. E. Lamont, C. Joshi, Y. Okawachi, F. W. Wise, M. Lipson, U. Keller, and A. L. Gaeta, *Opt. Lett.*, OL **40**, 5117 (2015).
- M. A. G. Porcel, F. Schepers, J. P. Epping, T. Hellwig, M. Hoekman, R. G. Heideman, P. J. M. van der Slot, C. J. Lee, R. Schmidt, R. Bratschitsch, C. Fallnich, and K.-J. Boller, *Opt. Express*, OE **25**, 1542 (2017).
- T. C. Briles, S.-P. Yu, T. E. Drake, J. R. Stone, and S. B. Papp, *Phys. Rev. Applied* **14**, 014006 (2020).
- H. Jung, S.-P. Yu, D. R. Carlson, T. E. Drake, T. C. Briles, and S. B. Papp, arXiv:2007.12958 [physics] (2020).
- L. V. R. Marcos, J. I. Larruquert, J. A. Méndez, and J. A. Aznárez, *Opt. Mater. Express*, OME **6**, 3622 (2016).
- M. Belt, M. L. Davenport, J. E. Bowers, and D. J. Blumenthal, *Optica*, OPTICA **4**, 532 (2017).
- M. Itoh, T. Kominato, M. Abe, M. Itoh, and T. Hashimoto, *Journal of Lightwave Technology* **33**, 318 (2015).
- C.-L. Wu, J.-Y. Huang, D.-H. Ou, T.-W. Liao, Y.-J. Chiu, M.-H. Shih, Y.-Y. Lin, A.-K. Chu, and C.-K. Lee, *Opt. Lett.*, OL **42**, 4804 (2017).
- R. Fan, C.-L. Wu, Y.-Y. Lin, C.-Y. Liu, P.-S. Hwang, C.-W. Liu, J. Qiao, M.-H. Shih, Y.-J. Hung, Y.-J. Chiu, A.-K. Chu, and C.-K. Lee, *Opt. Lett.*, OL **44**, 1512 (2019).
- J. R. C. Woods, J. Daykin, A. S. K. Tong, C. Lacava, P. Petropoulos, A. C. Tropper, P. Horak, J. S. Wilkinson, and V. Apostolopoulos, *Opt. Express*, OE **28**, 32173 (2020).
- K. F. Lamee, K. F. Lamee, D. R. Carlson, D. R. Carlson, Z. L. Newman, Z. L. Newman, S.-P. Yu, S.-P. Yu, S. B. Papp, and S. B. Papp, *Opt. Lett.*, OL **45**, 4192 (2020).
- L. Gao, F. Lemarchand, and M. Lequime, *Opt. Express*, OE **20**, 15734 (2012).
- “Commercial products are identified in this paper in order to specify the experimental procedure accurately. Such identification does not imply recommendation or endorsement by the National Institute of Standards and Technology, nor is it intended to imply that the products identified are necessarily the best available for the purpose.”
- S.-P. Yu, D. C. Cole, H. Jung, G. T. Moille, K. Srinivasan, and S. B. Papp, arXiv:2002.12502 [nlin, physics:physics] (2020).
- D. J. Moss, R. Morandotti, A. L. Gaeta, and M. Lipson, *Nature Photonics* **7**, 597 (2013).
- J. M. Dudley and J. R. Taylor, *Nature Photonics* **3**, 85 (2009).
- F. Leo, S.-P. Gorza, J. Safioui, P. Kockaert, S. Coen, U. Dave, B. Kuyken, and G. Roelkens, *Opt. Lett.*, OL **39**, 3623 (2014).
- N. Akhmediev and M. Karlsson, *Phys. Rev. A* **51**, 2602 (1995).
- D. D. Hickstein, G. C. Kerber, D. R. Carlson, L. Chang, D. Westly, K. Srinivasan, A. Kowligy, J. E. Bowers, S. A. Diddams, and S. B. Papp, *Phys. Rev. Lett.* **120**, 053903 (2018).
- D. R. Carlson, P. Hutchison, P. Hutchison, D. D. Hickstein, S. B. Papp, and S. B. Papp, *Opt. Express*, OE **27**, 37374 (2019).
- F. Vollmer and L. Yang, *Nanophotonics* **1**, 267 (2012).
- J. S. Levy, A. Gondarenko, M. A. Foster, A. C. Turner-Foster, A. L. Gaeta, and M. Lipson, *Nature Photonics* **4**, 37 (2010).
- S.-P. Yu, T. C. Briles, G. T. Moille, X. Lu, S. A. Diddams, K. Srinivasan, and S. B. Papp, *Phys. Rev. Applied* **11**, 044017 (2019).
- Y. K. Chembo and C. R. Menyuk, *Phys. Rev. A* **87**, 053852 (2013).

## FULL REFERENCES

- [1] X. Lu *et al.*, "Efficient telecom-to-visible spectral translation through ultralow power nonlinear nanophotonics," *Nature Photonics*, vol. 13, no. 9, Art. no. 9, Sep. 2019, doi: 10.1038/s41566-019-0464-9.
- [2] T. J. Kippenberg, A. L. Gaeta, M. Lipson, and M. L. Gorodetsky, "Dissipative Kerr solitons in optical microresonators," *Science*, vol. 361, no. 6402, Art. no. 6402, Aug. 2018, doi: 10.1126/science.aan8083.
- [3] A. S. Mayer *et al.*, "Frequency comb offset detection using supercontinuum generation in silicon nitride waveguides," *Opt. Express, OE*, vol. 23, no. 12, pp. 15440–15451, Jun. 2015, doi: 10.1364/OE.23.015440.
- [4] B. Kuyken *et al.*, "An octave-spanning mid-infrared frequency comb generated in a silicon nanophotonic wire waveguide," *Nature Communications*, vol. 6, no. 1, Art. no. 1, Feb. 2015, doi: 10.1038/ncomms7310.
- [5] D. D. Hickstein *et al.*, "Ultrabroadband Supercontinuum Generation and Frequency-Comb Stabilization Using On-Chip Waveguides with Both Cubic and Quadratic Nonlinearities," *Phys. Rev. Applied*, vol. 8, no. 1, p. 014025, Jul. 2017, doi: 10.1103/PhysRevApplied.8.014025.
- [6] D. Yoon Oh, K. Y. Yang, C. Fredrick, G. Ycas, S. A. Diddams, and K. J. Vahala, "Coherent ultra-violet to near-infrared generation in silica ridge waveguides," *Nature Communications*, vol. 8, no. 1, Art. no. 1, Jan. 2017, doi: 10.1038/ncomms13922.
- [7] B. Kuyken, M. Billet, F. Leo, K. Yvind, and M. Pu, "Octave-spanning coherent supercontinuum generation in an AlGaAs-on-insulator waveguide," *Opt. Lett., OL*, vol. 45, no. 3, pp. 603–606, Feb. 2020, doi: 10.1364/OL.45.000603.
- [8] K. Ikeda, R. E. Saperstein, N. Alic, and Y. Fainman, "Thermal and Kerr nonlinear properties of plasma-deposited silicon nitride/silicon dioxide waveguides," *Opt. Express, OE*, vol. 16, no. 17, Art. no. 17, Aug. 2008, doi: 10.1364/OE.16.012987.
- [9] K. S. Kim, R. H. Stolen, W. A. Reed, and K. W. Quoi, "Measurement of the nonlinear index of silica-core and dispersion-shifted fibers," *Opt. Lett., OL*, vol. 19, no. 4, Art. no. 4, Feb. 1994, doi: 10.1364/OL.19.000257.
- [10] K. Luke, Y. Okawachi, M. R. E. Lamont, A. L. Gaeta, and M. Lipson, "Broadband mid-infrared frequency comb generation in a Si<sub>3</sub>N<sub>4</sub> microresonator," *Opt. Lett., OL*, vol. 40, no. 21, Art. no. 21, Nov. 2015, doi: 10.1364/OL.40.004823.
- [11] A. R. Johnson *et al.*, "Octave-spanning coherent supercontinuum generation in a silicon nitride waveguide," *Opt. Lett., OL*, vol. 40, no. 21, Art. no. 21, Nov. 2015, doi: 10.1364/OL.40.005117.
- [12] M. A. G. Porcel *et al.*, "Two-octave spanning supercontinuum generation in stoichiometric silicon nitride waveguides pumped at telecom wavelengths," *Opt. Express, OE*, vol. 25, no. 2, Art. no. 2, Jan. 2017, doi: 10.1364/OE.25.001542.
- [13] T. C. Briles, S.-P. Yu, T. E. Drake, J. R. Stone, and S. B. Papp, "Generating Octave-Bandwidth Soliton Frequency Combs with Compact Low-Power Semiconductor Lasers," *Phys. Rev. Applied*, vol. 14, no. 1, p. 014006, Jul. 2020, doi: 10.1103/PhysRevApplied.14.014006.
- [14] H. Jung, S.-P. Yu, D. R. Carlson, T. E. Drake, T. C. Briles, and S. B. Papp, "Tantala Kerr-nonlinear integrated photonics," *arXiv:2007.12958 [physics]*, Jul. 2020, Accessed: Jul. 28, 2020. [Online]. Available: <http://arxiv.org/abs/2007.12958>.
- [15] L. V. R. Marcos, J. I. Larruquent, J. A. Méndez, and J. A. Aznárez, "Self-consistent optical constants of SiO<sub>2</sub> and Ta<sub>2</sub>O<sub>5</sub> films," *Opt. Mater. Express, OME*, vol. 6, no. 11, Art. no. 11, Nov. 2016, doi: 10.1364/OME.6.003622.
- [16] M. Belt, M. L. Davenport, J. E. Bowers, and D. J. Blumenthal, "Ultra-low-loss Ta<sub>2</sub>O<sub>5</sub>-core/SiO<sub>2</sub>-clad planar waveguides on Si substrates," *Optica, OPTICA*, vol. 4, no. 5, pp. 532–536, May 2017, doi: 10.1364/OPTICA.4.000532.
- [17] M. Itoh, T. Kominato, M. Abe, M. Itoh, and T. Hashimoto, "Low-Loss Silica-Based SiO<sub>2</sub>-Ta<sub>2</sub>O<sub>5</sub> Waveguides With Extremely High Δ Fabricated Using Sputtered Thin Films," *Journal of Lightwave Technology*, vol. 33, no. 2, pp. 318–323, Jan. 2015, doi: 10.1109/JLT.2014.2381644.
- [18] C.-L. Wu *et al.*, "Efficient wavelength conversion with low operation power in a Ta<sub>2</sub>O<sub>5</sub>-based micro-ring resonator," *Opt. Lett., OL*, vol. 42, no. 23, pp. 4804–4807, Dec. 2017, doi: 10.1364/OL.42.004804.
- [19] R. Fan *et al.*, "Visible to near-infrared octave spanning supercontinuum generation in tantalum pentoxide (Ta<sub>2</sub>O<sub>5</sub>) air-cladding waveguide," *Opt. Lett., OL*, vol. 44, no. 6, pp. 1512–1515, Mar. 2019, doi: 10.1364/OL.44.001512.
- [20] J. R. C. Woods *et al.*, "Supercontinuum generation in tantalum pentoxide waveguides for pump wavelengths in the 900 nm to 1500 nm spectral region," *Opt. Express, OE*, vol. 28, no. 21, pp. 32173–32184, Oct. 2020, doi: 10.1364/OE.403089.
- [21] K. F. Lamee *et al.*, "Nanophotonic tantala waveguides for supercontinuum generation pumped at 1560 nm," *Opt. Lett., OL*, vol. 45, no. 15, pp. 4192–4195, Aug. 2020, doi: 10.1364/OL.396950.
- [22] L. Gao, F. Lemarchand, and M. Lequime, "Exploitation of multiple incidences spectrometric measurements for thin film reverse engineering," *Opt. Express, OE*, vol. 20, no. 14, pp. 15734–15751, Jul. 2012, doi: 10.1364/OE.20.015734.
- [23] "Commercial products are identified in this paper in order to specify the experimental procedure accurately. Such identification does not imply recommendation or endorsement by the National Institute of Standards and Technology, nor is it intended to imply that the products identified are necessarily the best available for the purpose."
- [24] S.-P. Yu, D. C. Cole, H. Jung, G. T. Moille, K. Srinivasan, and S. B. Papp, "Spontaneous Pulse Formation in Edge-Less Photonic Crystal Resonators," *arXiv:2002.12502 [nlin, physics:physics]*, Feb. 2020, Accessed: Sep. 18, 2020. [Online]. Available: <http://arxiv.org/abs/2002.12502>.
- [25] D. J. Moss, R. Morandotti, A. L. Gaeta, and M. Lipson, "New CMOS-compatible platforms based on silicon nitride and Hydex for nonlinear optics," *Nature Photonics*, vol. 7, no. 8, Art. no. 8, Aug. 2013, doi: 10.1038/nphoton.2013.183.
- [26] J. M. Dudley and J. R. Taylor, "Ten years of nonlinear optics in photonic crystal fibre," *Nature Photonics*, vol. 3, no. 2, Art. no. 2, Feb. 2009, doi: 10.1038/nphoton.2008.285.
- [27] F. Leo *et al.*, "Dispersive wave emission and supercontinuum generation in a silicon wire waveguide pumped around the 1550 nm telecommunication wavelength," *Opt. Lett., OL*, vol. 39, no. 12, Art. no. 12, Jun. 2014, doi: 10.1364/OL.39.003623.
- [28] N. Akhmediev and M. Karlsson, "Cherenkov radiation emitted by solitons in optical fibers," *Phys. Rev. A*, vol. 51, no. 3, Art. no. 3, Mar. 1995, doi: 10.1103/PhysRevA.51.2602.
- [29] D. D. Hickstein *et al.*, "Quasi-Phase-Matched Supercontinuum Generation in Photonic Waveguides," *Phys. Rev. Lett.*, vol. 120, no. 5, Art. no. 5, Feb. 2018, doi: 10.1103/PhysRevLett.120.053903.
- [30] D. R. Carlson, P. Hutchison, P. Hutchison, D. D. Hickstein, S. B. Papp, and S. B. Papp, "Generating few-cycle pulses with integrated nonlinear photonics," *Opt. Express, OE*, vol. 27, no. 26, pp. 37374–37382, Dec. 2019, doi: 10.1364/OE.27.037374.
- [31] F. Vollmer and L. Yang, "Review Label-free detection with high-Q microcavities: a review of biosensing mechanisms for integrated devices," *Nanophotonics*, vol. 1, no. 3–4, pp. 267–291, Dec. 2012, doi: 10.1515/nanoph-2012-0021.
- [32] J. S. Levy, A. Gondarenko, M. A. Foster, A. C. Turner-Foster, A. L. Gaeta, and M. Lipson, "CMOS-compatible multiple-wavelength oscillator for on-chip optical interconnects," *Nature Photonics*, vol. 4, no. 1, Art. no. 1, Jan. 2010, doi: 10.1038/nphoton.2009.259.
- [33] S.-P. Yu *et al.*, "Tuning Kerr-Soliton Frequency Combs to Atomic Resonances," *Phys. Rev. Applied*, vol. 11, no. 4, Art. no. 4, Apr. 2019, doi: 10.1103/PhysRevApplied.11.044017.
- [34] Y. K. Chembo and C. R. Menyuk, "Spatiotemporal Lugiato-Lefever formalism for Kerr-comb generation in whispering-gallery-mode resonators," *Phys. Rev. A*, vol. 87, no. 5, Art. no. 5, May 2013, doi: 10.1103/PhysRevA.87.053852.